Journal of ELECTRONIC MATERIALS, Vol. 49, No. 5, 2020
https://doi.org/10.1007/s11664-020-07995-1
© 2020 The Minerals, Metals & Materials Society

Remarkable Electrical Conductivity Enhancement Through Mutual Variation of MWCNTs/Tin Oxide Concentration: Structural, Morphological and Electrical Properties

MAGDA D. BADRY,[1] MOHAMMED A. WAHBA ,[2,4] RABAB K. KHALED,[1] and SAFAA K. EL-MAHY[3]

1.—Department of Physical Chemistry, National Research Centre, El-Behoos St., Dokki, Giza, Egypt. 2.—Department of Inorganic Chemistry, National Research Centre, 33 El Bohouth st. (former Eltahrir st.), Dokki, Giza 12622, Egypt. 3.—Department of Physics, Faculty of Women for Arts, Science and Education, Ain Shams University, Cairo, Egypt. 4.—e-mail: mohamedwahba12@gmail.com

Tin oxide/MWCNTs hybrid nanocomposites were synthesized via the malic acid-assisted modified sol–gel method. Effect of the concentration variation of both MWCNTs and tin oxide on the hybrid nanostructure, morphology, thermal and optical properties was studied using spectroscopic and analytical tools including: thermal gravimetric analyses (TGA), x-ray diffraction (XRD), scanning electron microscope (SEM), transition electron microscope (TEM), and ultraviolet–visible (UV–Vis) spectroscopy. Thermal gravimetric analyses of the hybrid nanocomposites showed a mode of stability up $\approx 375^{\circ}C$, after this temperature the sample is subjected to decomposition of the MWCNTs. XRD patterns of the pristine tin oxide sample showed the presence of characteristic peaks related to two crystalline phases of tin oxide (rutile SnO_2 and orthorhombic SnO), while the hybrid CSn10 (synthesized via 10% weight substitution of MWCNTs by tin oxide) and SnC10 (synthesized via 10% weight substitution of tin oxide by MWCNTs) nanocomposites showed a clear decrease in the crystallinity as a proof for dispersing of tin oxide nanoparticles within the hollow cavity of MWCNTs, which was further confirmed by SEM and TEM images. Furthermore, a complete absence of the characteristic peak of orthorhombic SnO was observed in the CSn10 sample. Optical and electrical properties of the hybrid nanocomposites-chitosan thin films were investigated before and after exposing to UV radiation for 1 h. The UV–Vis spectra showed a blue shift upon introducing MWCNTs into the oxide matrix while prolonged exposure to UV-radiation markedly affected the absorption and the band gaps of all nanocomposites. Investigation of the electric properties interestingly showed remarkable electrical conductivity enhancements upon introducing either MWCNTs or tin oxide in the matrix of each other. Introducing 10% MWCNTs into the tin oxide structure (SnC10) was accompanied by 76-fold increase in the electric conductivity; while incorporating 10% of tin oxide (CSn10) was accompanied by 110-fold increase in the electric conductivity of MWCNTs at 100 Hz frequency. Furthermore, the effect of prolonged UV-radiation on the electric properties of the synthesized hybrid nanocomposites was also reported.

Key words: MWCNTs/tin oxide hybrid nanocomposites, structural, morphological, uv radiation, optical and electrical properties

(Received October 23, 2019; accepted February 1, 2020; published online February 12, 2020)

INTRODUCTION

In the last two decades, carbon nanotubes (CNTs) have established a revolutionary change in scientific research and have opened up a broad range of possible research and functional applications due to their superior behaviors and interesting properties over other materials.[1–3] Carbon nanotubes appear to be the most promising because of their unique chemical, physical and electrical properties. The high electrical conductivity and mechanical strength as well as the chemical inertness and the large aspect ratio are vital traits of MWCNTs that provide a great improvement in electrical properties such as: threshold field, turn-on field, and emission current stability.[4] The quantum confining of electrons due to the nanotubes size endows this unique class of materials exceptional electronic properties and sets them as perfect candidates for electronic applications. For instance, CNTs have been testified as outstanding field emitters at low working voltages.[5] Surface modification of CNTs can lead to looked-for changes in the electrical character of CNTs. These modifications could be achieved via decorating with metal and metal oxides which causes anticipated-improvement in the electrical conductivity and, consequently, enhancement of the field emission and the whole of the electrical properties.[6,7]

Multi-walled CNT/metal oxide (MWCNTs/MO) hybrid nanocomposites represent a new class of compounds with fascinating properties that not only merge the characteristics of carbon nanotubes and metal oxides but also grasp novel rewards triggered by metal oxide–carbon nanotubes interactions.[6,8] Furthermore, the harmonious combination of the materials could provide effective solutions for some drawbacks that hinder successful practical use of each of them separately. For example, the agglomeration of nanosized metal oxide represents a major challenge as a direct result to unsatisfied valence on the immobilized metal atoms that leads to atom–atom dangling bonds. Dispersion of nanosized metal oxide particles on functionalized carbon nanotubes prevents the problem of agglomeration. In addition, CNTs can perform as carrier and play a crucial role in stabilization and maintaining their integrity for these nanoparticles. Consequently, these hybrid nanocomposites draw much attention in multifunctional applications such as: environment remediation, optics, electronic, and mechanics compared with the isolated nanoparticles.[9–12] They can act as effective sorbents to tackle environmental pollution due to their chemically inertness and high surface area that provide more effective adsorption sites that are perfect for physical adsorption.[13] Moreover, they have been widely used to support and enhance the catalytic activity of metal oxides.[12]

Tin dioxide is considered one of the most recognized n-type semiconductors. Its remarkable carrier concentration (up to $6 \times 1020\ cm^{-3}$) as well as the wide bandgap (about 3.6 eV) are important characteristics for various applications such as: gas sensors,[14] solar cells,[15] lithium ion batteries,[16] and cathode emitters of the FE device.[17] Hybrid MWCNTs/SnO_2 nanocomposites could show innovative electronic properties different from those of the separate components. This prediction relies basically on the finite Schottky barrier between MWCNTs and SnO_2 and the fact that the work function of both of them is nearly equal.[18] This sustains the nanocomposite's unique electrical properties as the electrons could travel easily through the SnO_2 grains to carbon nanotubes and then promote efficient conductivity in their nanocomposites. Several techniques have been used to synthesize hybrid MO/MWCNTs nanostructures, such as electro deposition, hydrothermal treatment with supercritical solvents, plasma treated and atomic layer deposition (ALD), and chemical deposition (CVD) under oxygen-free environments[11,19–21] as well as physical deposition using electron beam deposition, laser ablation, sputtering and thermal evaporation.[2,22–24] However, these techniques incorporate expensive and time consuming procedures. Most of these drawbacks could be overcome using the sol-gel method.[25,26] It is simple, economic, time saving and can be achieved at lower temperature and with no pressure and no need for expensive equipment. In this work, SnOx/MWCNTs hybrid nanocomposites were synthesized via a malic acid-assisted modified sol–gel method. Effect of the mutual MWCNTs/SnO_2 substitution on the hybrid nanostructure, morphology, thermal and optical properties as well as their electric properties were also investigated using spectroscopic and analytical techniques. Furthermore, the effect of prolonged UV radiation on the electric properties of the synthesized hybrid nanocomposites was also reported.

EXPERIMENTAL

Functionalization of MWCNTs

The raw MWCNTs employed in this work were supplied by Sigma Aldrich. To make the carbon nanotubes amenable to aqueous processing, firstly, purification of carbon nanotubes was performed with hydrochloric acid (HCl) to remove impurities from structure. Afterward, MWCNTs were functionalized by suspension of 5 gm of MWCNTs in 350 mL acid mixture of HNO_3 (65%): H_2SO_4 (98%) (1:3 v/v) then refluxed for 12 h, then filtered from acid solutions and washed with deionized water several times until neutral pH, and then dried in an oven at 80°C.[27]

Preparation of SnO_2

$SnCl_2{\cdot}2H_2O$ was used as a precursor for preparation of SnO_2 by the sol–gel method after removing chloride ions. It is well known that the residual chlorine ions are very difficult to rinse out.[28] For

this purpose, firstly, 8.0 mmol $SnCl_2{\cdot}2H_2O$ was dissolved in deionized water then, a stoichiometric ratio of NH_3 (25%) solution was added. After the precipitation of tin as hydroxide, the solid was filtered and washed with doubly distilled water and diluted NH_3 solution until negative $AgNO_3$ test for chloride was attained; the final precipitate was used as the tin precursor. The final precipitate was dissolved in a solution of 8.0 mmol of malic acid, then 5 ml of ethylene glycol added to the solution in order to form a complex with the tin cation. The carboxylic acid acts as a fuel during the formation process of metal oxide powders, decomposes the homogenous precipitate of metal complexes at low temperature, and yields the free impurity samples. The stirring was continued for 1 h at 80°C. Ammonia solution was then added drop-by-drop to these solutions with constant stirring. Addition of the diluted basic solution (typically NH_4OH) speeds up the hydrolysis process. The acidity of the sol is neutralized slowly to pH 7, which stimulates the gelatin process. At this stage a mechanically unstable "wet" gel is formed. The prepared solution was then evaporated at 70–80°C with magnetic stirring for about 6 h until a transparent xerogel was obtained. The resulting xerogel precursor was decomposed at 500°C for 6 h in air to eliminate the organic substances, and naturally cooled to room temperature by turning the furnace off. The decomposed powders were slightly ground using a mortar and naturally cooled to room temperature.

Preparation of SnOx-MWCNTs Nanocomposites

MWCNTs/MO composites can be prepared by various methods, here, the focus was on a wet chemistry method where the MWCNTs act as nucleation sites for the tin oxide. A 10-gram ratio of SnO_2: MWCNTs: was used to prepare SnO_2@MWCNTs nanocomposites. (0.15 g, 1 mmol) of tin hydroxide in glacial acetic acid was added drop-wise to a continuously stirred aqueous solution of (0.13 g, 1 mmol) malic acid and 5 ml ethylene glycol. Then, 1.5 g of acid functionalized MWCNTs was added to the solution that was left under stirring for 1 h. After that, ammonia solution 25% was slowly added to this solution with keeping a constant stirring. The acidity of the sol was neutralized slowly to pH 7. The prepared solution was then evaporated at 70–80°C with magnetic stirring for about 6 h until a xerogel was obtained. The resulting xerogel precursor was decomposed at 375°C for 6 h in air to eliminate the organic substances, and naturally cooled to room temperature by turning the furnace off. The decomposed powders were slightly ground using a mortar and naturally cooled to room temperature. This sample was coded CSn10. The same procedures were followed to synthesize MWCNTs@SnO_2 nanocomposite with 1 MWCNT: 10 SnO_2 gram ratio and coded SnC10.

CHARACTERIZATION

Characterization of the nanocomposites samples was done using the thermogravimetric analysis that was conducted using a Perkin-Elmer Delta series (TGA7) thermosanalyzer. X-ray diffraction (XRD) with a Bruker D8 Advance diffractometer was done using Cu monochromatized Cu Kα radiation of a Bruker 8 advance diffractometer. The average crystallite size (D) of the nanocomposites was calculated from the half height line broadening by applying the Scherrer formula.[29] SEM-Energy Dispersive x-ray spectroscope (EDX) measurements were recorded on a scanning electron microscope (FESEM, FEI Nova-Nano SEM-600, the Netherlands). Transmission electron microscopy (TEM) images were obtained by using a JEM-2100 transmission electron microscope (Japan Electron Optics Laboratory Co. Ltd., Tokyo, Japan) operating with an accelerating voltage of 100 kV. Optical measurements were recorded on the UV lamp (254 nm). Electrical measurements were obtained using a HIOKI Japan 3532-50 LCR HI TESTER.

Dielectric Measurements

An appropriate amount of (functionalized MWCNTs; SnO_x; SnC10 and CSn10 samples) was dissolved in CS solution at 70–80°C for 1 h and ultrasonicated for 1 h. Finally, the mixture was poured into Petri dishes, followed by solvent evaporation at room temperature to form the films. Electrical measurements were performed in the frequency range from 10^2 Hz to 10^6 Hz, by using a HIOKI Japan 3532-50 LCR HI TESTER. The dielectric constant was calculated at each frequency by the formula $\varepsilon' = \frac{Cd}{\varepsilon_o A}$, where$\varepsilon'$ is the relative permittivity or dielectric constant, C and d are the capacitance and thickness of nanocomposites films, ε_o is the dielectric constant of vacuum (8.85×10^{-12} F/m) and A is the area of the electrode. The dielectric loss (ε'') is calculated from the relation: $\varepsilon'' = \varepsilon' * D$, where D is the dielectric loss tangent or the dissipation factor is measured by a LCR meter at different frequencies. The ac electrical conductivity of nanocomposites films was calculated according to the equation $\sigma_{ac} = L/RA$, where R is the electrical resistance, L is the thickness of nanocomposites films and A is the area of the electrode.

RESULTS AND DISCUSSION

Thermal Gravimetric Analysis (TGA)

It was reported that MWCNTs materials are subject to decomposition by heat treating around 550°C.[30–32] TGA was carried out in order to choose the right heat-treated temperature for formation

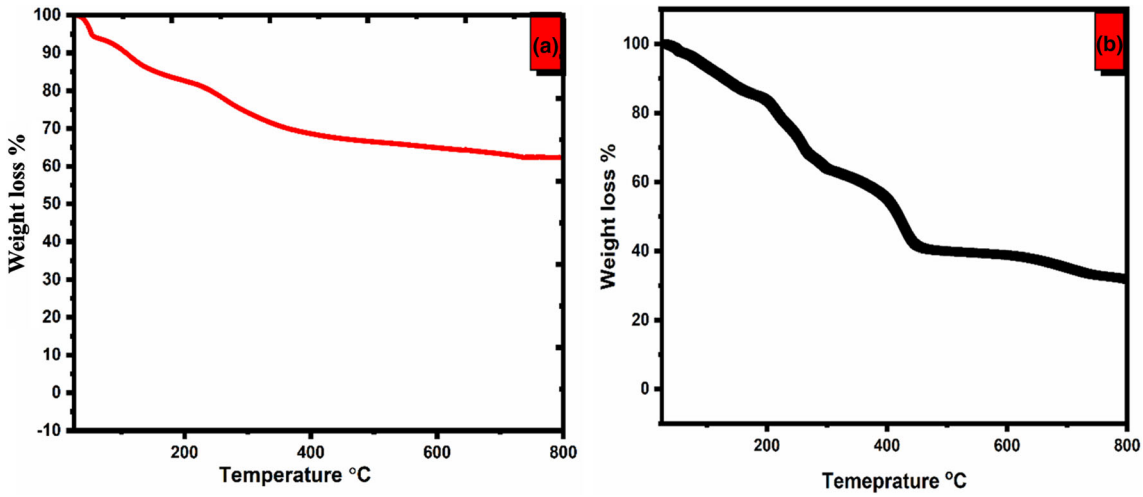

Fig. 1. TGA thermograph of the hybrid nanocomposites (a) SnC10 and (b) CSn10.

the metal oxides as well as the MWCNTs/MO nanocomposites. TGA curve of SnC10 and CSn10 nanocomposites conducted in air is shown in Fig. 1. The weight loss around 125°C is due to the physio-adsorbed water. Both patterns show weight loss in a range of 200–400°C due to loss of organic matter (malic acid and ethylene glycol) as well as partial oxidation of MWCNTs. In contrast to the SnC10, a massive weight loss of nearly 25% was observed for CSn10 in the range of 400–686°C, which can be rendered to oxidation of the remaining amorphous carbon and decomposition of the remaining organic carboxylic acid matter.[33] The thermogram figures show mode of stability up ≈ 375°C, after this temperature the sample is subjected to decomposition of the MWCNTs. This observation is further supported by changing of the color of the sample from dark black to pale whitish grey. Under isothermal conditions, the walls of MWCNTs started to deteriorate and form bundles at 400°C in air; it was reported by Bom et al. that oxidation of raw MWCNTs starting at 420°C and finished at 630°C while Mahajan et al. demonstrated that oxidation of graphitized MWCNTs took place between 650°C and 870°C.[34,35] The temperatures at which MWCNTs are burnt in our samples are in fact lower than that of pristine MWCNTs reported in the literature.[30,31] These findings can be explained by the oxidation ability of the tin oxide component, which helps in removing the carbon content at lower temperatures.[36]

X-Ray Diffraction Analysis (XRD)

The obtained products were characterized by XRD in order to confirm the formation metal oxide nanoparticles on MWCNTs as shown in Fig. 2. The diffraction pattern of the pristine-free MWCNT sample shows characteristic peaks at 2θ = 26.04°, 43.15°, 51.81° indexed to the (002), (100) and (004)

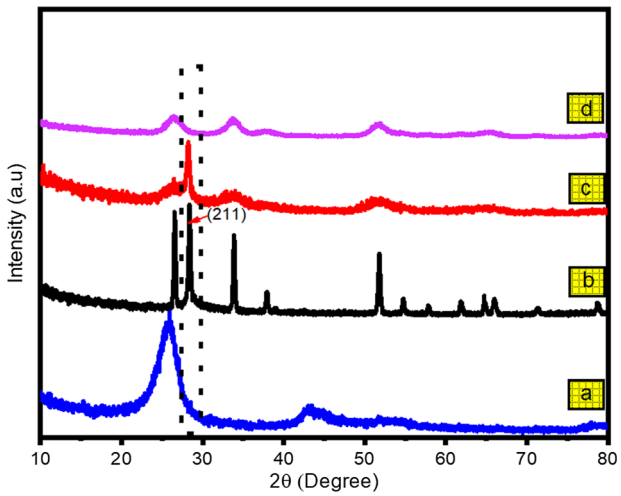

Fig. 2. XRD of (a) functionalized MWCNTs; (b) SnO_x; (c) SnC10 and (d) CSn10 samples.

planes (JCPDS no. 41- 1487),[37] respectively. The pristine tin oxide sample showed well diffraction peaks indexed to the tetragonal rutile structure of SnO_2. The well-defined broad reflections observed in the XRD pattern at 2θ = 26.51°, 33.67°, 37.92°, 51.70°, 54.83°, 57.8°, 61.88°, 64.93°, 66.04°, and 78.63° corresponded well to (110), (101), (200), (211), (200), (002), (130), (112), (301) and (202) planes, respectively, which are in good agreement with the previously reported,[38] and match well with Entry # 96-100-0063, COD-1000062 confirming the formation of a polycrystalline SnO_2. The estimated values of the lattice constants and unit cell volume (V) were obtained from Rietveld refinement analysis using FULLPROF software[27] and were found to be a = b = 4.734 Å and c = 3.185 Å. The spectrum showed an additional peak at 2θ = 28.36 related to (112) plane of orthorhombic SnO indicating its presence in the sample COD ID 110-0021 96-110-0021.[39]The

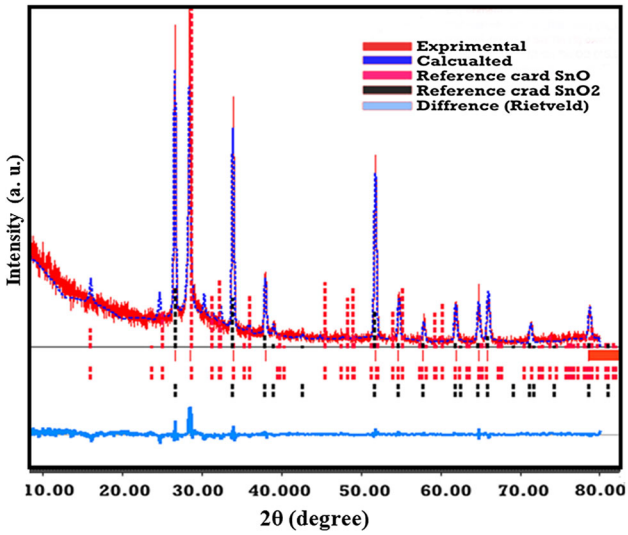

Fig. 3. Rietveld refinement of SnO_x pattern using full proof software.

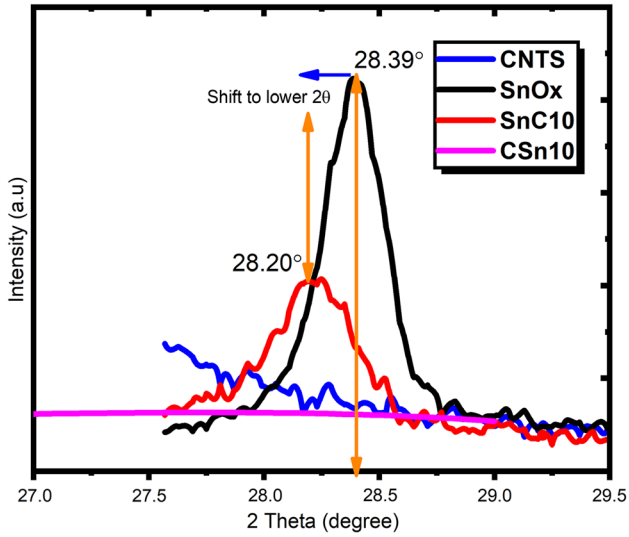

Fig. 4. Enlarged pattern for the main peak (211) of the orthorhombic phase of SnO sample prepared by calcination at 500°C.

Rietveld refinement pattern revealed a good fitting between the experimental and the calculated profiles for the two phases of tin oxide Fig. 3. The phase ratio of SnO_2 and SnO was found to be 70.1: 29.9. The average crystallite size of the synthesized nanostructures was calculated by measuring the full-width at the half-maximum (FWHM) of the most intense four peaks using diffraction peaks and using the Debye–Scherrer equation ,and it was found to be 30.1 nm, 6.6 nm and 4.5 nm for pristine SnOx, SnC10 and CSn10, respectively (Fig. 4).

The diffraction pattern of SnC10 nanocomposite showed a decrease in the intensity of the main characteristic peaks of SnO_x; the reason for this observation is that these peaks are overlapped by the diffraction peaks of MWCNTs inserted in the sample.[40] For instance, the main peak of MWCNTs at 26.06° masked the main peaks at 26.04 of tin oxide since their positions are so close. The decrease in the crystalline extent of tin oxide in the SnC10 than the crystalline extent of the pristine oxide is a good proof for good dispersing of some of the metal oxide nanoparticles within the hollow cavity of MWCNTs which results in shielding of the peaks of metal oxides by MWCNTs. These findings are further supported by the scanning and the transition electron microscope images (Figs. 5, 7). Also, a noticeable shift to a lower 2θ angle in the (112) plane was observed in the SnC10 sample (Fig. 2). These shifts could be assigned to possible substitution of some Sn atoms with MWCNTs particles with a size higher than the ionic radius of Sn^{4+} and Sn^{+2} as a result of the insertion of MWCNTS into the SnO_x lattice.[41,42] In the CSn10 pattern, the MWCNTs diffraction peaks became more prominent as a result of the higher content of MWCNTs. This is accompanied by more broadening and disappearance of the SnO_2 main diffraction peaks in addition to the absence of the characteristic peak of orthorhombic SnO.

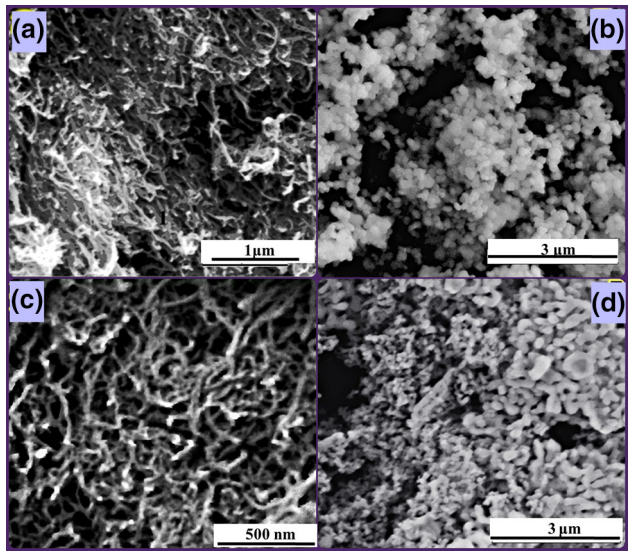

Fig. 5. SEM images of (a) functionalized MWCNTs; (b) SnO_x; (c) SnC10 and (d) CSn10 samples.

SEM–EDX

Scanning electron microscopy (SEM) images of the synthesized pure as well as the tin oxide/ MWCNTs hybrid nanocomposites are presented in Fig. 5. A typical morphology of functionalized MWCNTs with diameters oscillated between 15–20 nm and lengths ranged between 3 and 6 μm. It can be observed that the functionalized-MWCNTs have a random orientation after acid treatment. This tangled orientation could be related to the attached carboxylic groups onto the surface of MWCNTs and an indicative of defects in their structure. The morphology of the pure tin oxide nanoparticles (Fig. 5b) adopts a spherical shape with a nearly uniform nano-size. It was observed also the particles are agglomerated. This

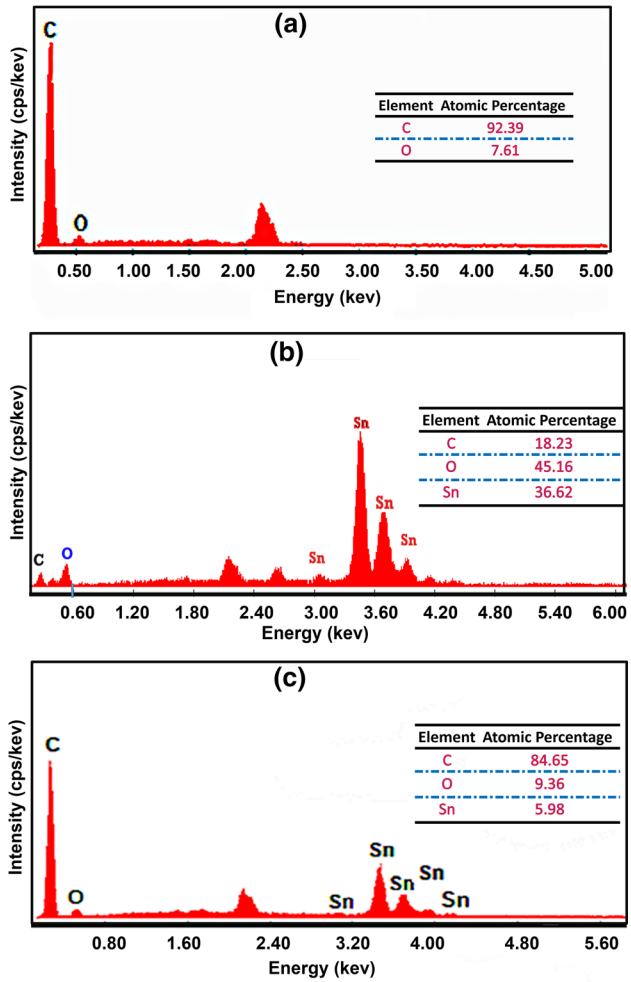

Fig. 6. EDX of (a) functionalized MWCNTs, (b)SnC10 and (c)CSn10 samples.

agglomeration is related to nanosize of the particles and consistent with particle size estimated from XRD patterns (Fig. 2); as the particle size decreases and go towards the nanoscale, the agglomeration of particles increases. The morphology of CSn10 and SnC10 (Fig. 5c, d) reveals that many nanoparticles are effectively anchored on the sidewall of the MWCNTs both in the two nanocomposites. Energy dispersive x-ray spectroscope (EDX) measurement was used for elemental identification and quantitative composition of samples. Figure 6a represents the EDX of the oxidized MWCNTs, and shows the presence of oxygen in the sample in addition to the carbon element, which suggests successful acid oxidation of the MWCNTs surface and the presence of oxygen-containing groups such as carboxyl (-COOH) and hydroxyl (-OH) that could be used as subsidiary sites for addition reaction or further functionalization. Figure 6b shows EDX analysis of the CSn10 nanocomposite was performed and indicated the atomic content of SnO_x in the sample. It can be concluded that the composite consists of SnO_x particles and MWCNTs to form a hybrid nanocomposite. Taken together SEM, TEM and EDX data clearly point toward a good distribution of Sn, O and C. EDX data indicates that the amounts of Sn and O are highly smaller than C in the SnC10 sample, while the carbon element is prominent in the CSn10, which is closely related to the atomic percentage ratio used in the preparation procedures (Fig. 7).

TEM

To further study the structure of composites, transmission electron microscopy (TEM) was done to examine the present state and the nanostructures of the synthesized nanocomposites. The observed average width of MWCNT was about 15 nm while the lengths extended to several microns. It is found also that SnO_x nanoparticles are homogeneously dispersed on the surface of MWCNTs on both of two composite samples (CSn10, SnC10) with an average particle size ranging between 4–5 nm and 3–4.5 nm, respectively. The small discrepancy in crystallite size (calculated from XRD) and the particle size could be related to the formation of an amorphous layer on the nanocrystals which is commonly observed in nanoparticle systems.[41,43] It was also observed that the SnO_x particles are not only formed on the surface but also nucleated and have growth within the MWCNTs that still preserve their tube shape, and this could be a reason for the apparent small particle size. MWCNTs/SnO_x bondings can be formed naturally through some physicochemical interactions such as Van der Waals forces, H bonding and other bonds. For example, the OH group on the metal oxide/hydroxide polymeric network may possibly react with the OH and COOH groups on the functionalized MWCNTs and, thus, the bonding through C-O-Sn or O=C-O-Sn might form through the dehydration reaction that happens among the groups on the two materials. The absorbed SnO_x on the MWCNTs would grow up and enclose the MWCNTs during the heat-treatment, which indicated that SnO_x had infiltrated into the MWCNT and filled the interior. The nucleation is promoted by heterogeneous nucleation and also contributed by the defect on the MWCNTs surfaces caused by functionalization with the HNO_3 (65%) and H_2SO_4 (98%) (1:3 v/v) acid mixture.

Optical Properties

The UV–Vis absorption spectra of the synthesized pure- and hybrid-nanocomposites-chitosan (CS) thin films before and after exposure to UV radiation for 1 h are shown in Fig. 8. The measurements of absorption spectra were carried out at room temperature and wavelength ranging from 200 nm to 800 nm. It is observed that all samples exhibit two characteristic peaks in (230–240) and (301–305) nm characteristic of multi-walled CNTs and chitosan, respectively.[44] Whereas, the MWCNTs/CS nanocomposites showed an additional absorption

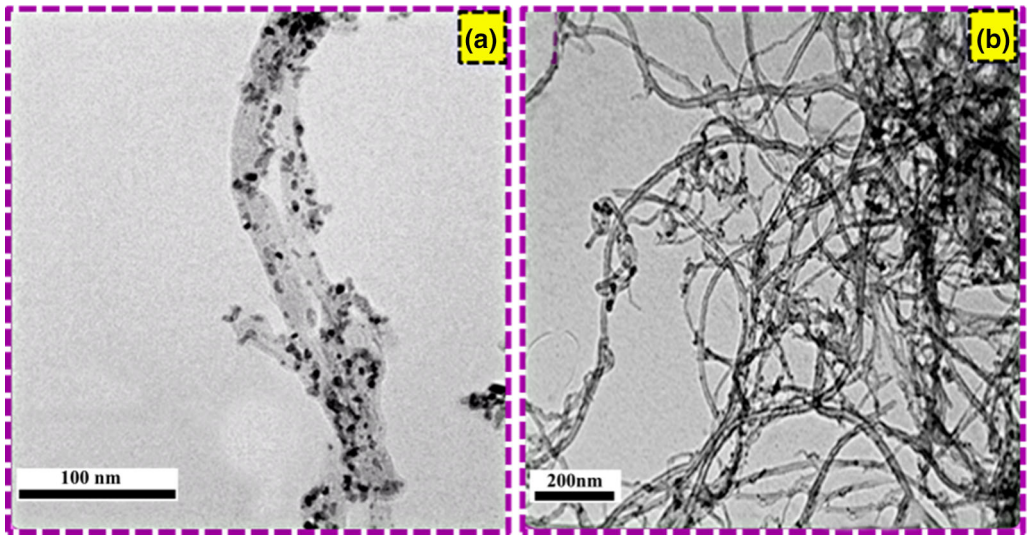

Fig. 7. TEM images of (a) SnC10 and (b) CSn10 hybrid nanocomposites.

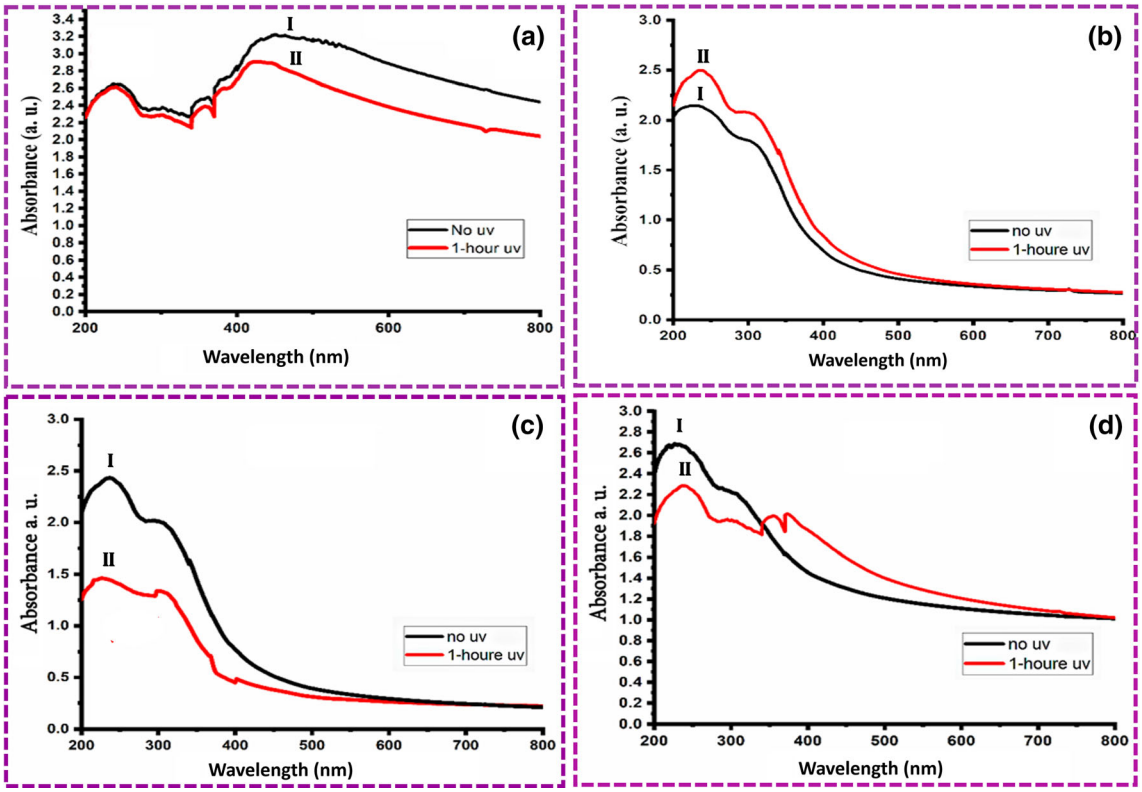

Fig. 8. UV-Vis spectrum of chitosan thin films with (a) functionalized MWCNTs; (b) SnO_x; (c) CSn10 and (d) SnC10; before (I) and after 1-h (II) exposure to UV radiation.

peak at 452 nm. It was noticed that both MWCNTs/CS nanocomposite and SnO_x/CS nanocomposite demonstrate an opposite response upon prolonged exposure to UV-radiation. As can be seen, the spectra revealed a decrease in the absorbance intensity with increasing the exposure time in MWCNTs/CS nanocomposite, while an increase in the absorbance intensity was observed in SnO_2/CS nanocomposite. Also, a prolonged exposure of the hybrid nanocomposites to UV radiation displays interesting variation response in both SnC10 and CSn10 samples. For SnC10, a decreasing in the absorption intensity was observed up to $\simeq$ 550 nm. On the other hand, the CSn10 sample showed an apparent decline in the absorption intensity in the (200–350 nm) range whereas a pronounced

enhancement in the absorption was perceived in the (350–600 nm) range. A significant red shift accompanied by the appearance of new absorbance peaks at 350 nm and 370 nm was observed which could be related to the MWCNTs higher content in this sample. These findings are supported by Savage and Grujicic who demonstrated that the carbon nanotubes exhibit photo-induced oxidation of the nanotubes when exposed simultaneously to UV light and oxygen.[45,46] A blue shift was also noticed upon introducing MWCNTs into the oxide matrix. This shift could be due to interaction of MWCNTs with the tin oxide as well as redistribution of polar and localized state density within the band gap of the metal oxides due to the impact of MWCNTs.[47] The measurement of the band gap of materials is important in the semiconductor, nanomaterial and solar industries. The optical band gap of the samples is determined from the absorption spectra near the absorption edges using the equation: $Eg(\mathrm{eV}) = hc/\lambda$, where h is Planck's constant ($6.626*10^{-34}$ Js); C velocity of light ($3*10^{8}$ m/s); and λ is the wavelength (m). The optical band gap values of the samples before and after exposing to UV–Vis radiation are listed in Table I. It can be noticed that the value of band gap for MWCNTs/CS nanocomposite is lower than that of its nanocomposites with metal oxide as well as the pristine metal oxide (tin oxide of $\sim$ 3.30 eV).[48,49] The band gap values indicate a decline by increasing the MWCNTs content in nanocomposites that can be assigned to the interaction of MWCNTs with the metal oxides bands, which creates sub-band states in the metal oxide band gap accompanied by a narrowing of the band gap.[50] Moreover, upon introducing MWCNTs, the degree of amorphous nature in the nanocomposites increased as asserted from the XRD pattern (Fig. 2). Due to the structural disorder in these amorphous materials, a dense localized state can exist between valence and conduction bands (Urbach energy or the Urbach tail). It was reported that the Urbach energy increases with the MWCNTs, which results in a rise of localized state formation through the metal oxide bands and leads to a decrease in the band gap energies.[51] Also, we can notice that, *Eg* values of the synthesized hybrid nanocomposites SnC10 and CSn10 decrease upon exposure to UV-radiation. This can be attributed to the structural sensitivity of these materials to UV-radiation. Upon exposure to UV-radiation, electron–hole pairs could be generated and spatially separated in SnO_x/MWCNTs matrix-structure which consequently plays a role in the diminishing of the band gap values.[52]

Table I. The optical band gap values (*Eg*/ev of the samples before and after exposure to UV radiation

Nanocomposites	0 h	1 h
MWCNTs/CS	0.92	1.236
SnO_2/CS	3.10	2.80
SnC10	2.82	2.60
CSn10	2.75	2.20

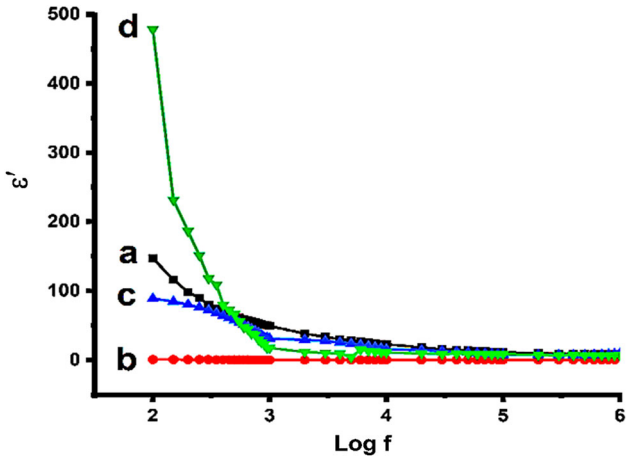

Fig. 9. Dielectric constant of chitosan thin films of (a) functionalized MWCNT; (b) SnOx; (c) SnC10 and (d) CSn10.

Electrical Properties

Figure 9 shows the dielectric constant as a function of frequency at room temperature for the pure and the hybrid nanocomposites samples. It is clearly observed that the ε' values for the nanocomposites monotonously declines with increasing the frequency up to 10^4 Hz, while ε' values at higher frequencies endure nearly a constant value. One reason for this is that the escalation of frequency was accompanied by a diminution in polarization till reaching a constant value. Generally, in the low frequency range, the long polarization time as well as the space charge polarization has a significant role in the composites due to the existence of various types of polarization mechanisms like electronic, ionic, orientation and space-charge polarization.[53] This leads to large values of dielectric constant at low frequencies. The implementation of an electric field results in moving of the space charges and creation of dipole moments, which is called space-charge polarization. Furthermore, the applied field leads to rotation of these dipole moments and resulting in polarization rotation that contributes in these high dielectric values .[54] Above a specific frequency, the hopping between different metal ions and charges are not able to follow the alternating field. At this point the charge carriers start to move and the dielectric constant declines to a small value before the field reversal occurs.[55] A great difference in the dielectric constant values of the synthesized was detected in the low frequency range 10^2–10^4 Hz among all the samples. At 100 Hz, the dielectric constant of SnC10 nanocomposite recorded 89.13, which is about 115 times greater than SnOx (ε' = 0.77), whereas incorporation of 10% tin oxide

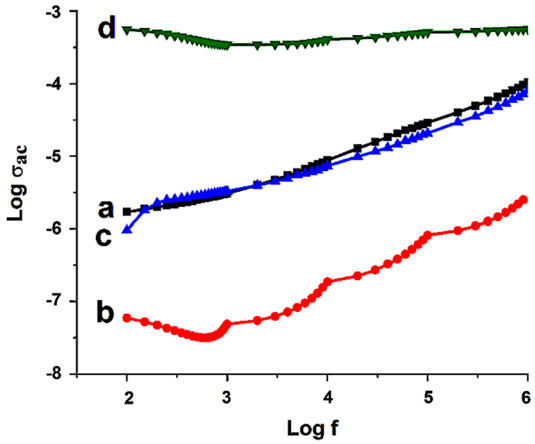

Fig. 10. The relation between Log σ_{ac} and log f of chitosan thin films of (a) functionalized MWCNT, (b) SnO_x, (c) SnC10 and (d) CSn10 nanocomposites.

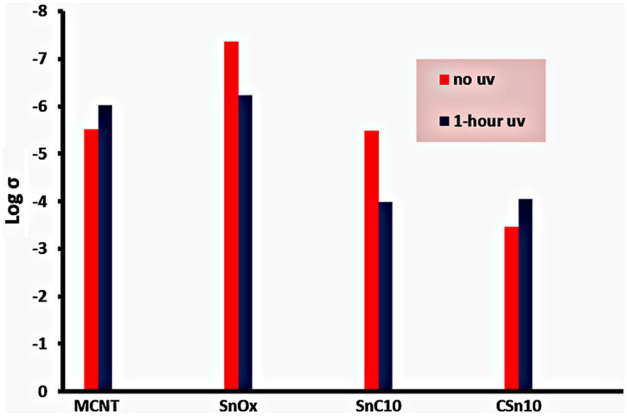

Fig. 11. Variation of Log σ_{ac} for functionalized MWCNTs; SnO_x; SnC10 and CSn10 samples at 0, 1 h exposure to UV.

in MWCNTs (CSn10) leads to a three fold increase in the dielectric constant from 147.57 to 478.38. In the low frequency range, the dielectric permittivity is enormous and rises with increasing MWCNTs concentration in the composites.[56] On the other hand, such differences in the dielectric constant values vanish at higher frequency $> 10^4$ range, and all samples showed small dielectric values, which shows the capability of these materials to be used for high frequency in such as photonic, ferroelectric and electro-optic applications.

Figure 10 shows the frequency dependence of conductivity for all the four samples at room temperature. In the low frequency range up to 10^3 Hz, both pure SnO_2 and CSn10 show slight decreasing in log σ_{ac} with increasing the frequency, whereas MWCNTs and SnC10 presents slight increases in the same range. On the contrary, at high frequencies $> 10^3$ region, there is an abrupt increase in the conductivity, and it is enormous at high frequency, which could be attributed to the occurrence of short range hopping conduction at the surface of the hybrid nanocomposites.[57] Either incorporating of 10% of MWCNTs in the tin oxide matrix or incorporating 10% tin oxide in the MWCNTs have a great effect on enhancement of the electrical property of both tin oxide and MWCNTs. Compared with the undoped SnO_2 nanoparticles, the conductivity of SnO_x doped with 10% wt carbon nanotubes (SnC10) increased by a factor of about 76 times; on the other hand, the CSn10 demonstrated a significant enhancement in the electric conductivity of MWCNTs by 110 times. One possible explanation for such higher electric conductivity in the SnO_2/MWCNTs hybrid nanocomposites could be related to the very low Schottky barrier between SnO_2 grains and MWCNTs, so electrons can easily travel between them. In addition, electrons conduct in the MWCNTs with a low resistance. Furthermore, the high aspect ratio structure and good conductivity of MWCNT-COOHs make them act as electrons-bridges linking SnO_x nanoparticles together. The numerous p-orbits of MWCNT-COOHs also can act as acceptor levers to improve the conductivity of SnO_2.[58]

The UV exposure also has a great effect on the electrical properties of the synthesized MWCNTS/ SnO_2 nanocomposites. Figure 11 shows the variation in the electric conductivity of the samples in before and after 1 h of UV illumination. It was observed that both SnC10 and CSn10 adopt a reverse response to the UV illumination regarding the electric conductivity. The SnC10 sample (doped with 10% MWCNTs) showed a marked enhancement in electric conductivity, while the electric conductivity with high MWCNTs content (CSn10) recorded a marked decreased value. These findings are very consistent with the values recorded for pure MWCNTs and SnO_2 upon 1 h UV exposure: in the time that pure SnO_2 showed an enhancement in the electric conductivity by about ten times, MWCNTS showed a decrease by about two thirds of its electric conductivity. From these results, it can be deduced that both SnC10 and CSn10 showed an electric-UV response reliant greatly on their element content. One possible explanation for such a conductivity decrease in CSn10 suggests that, in a rich oxygen environment, UV-light radiation can prompt ozone formation, which induces a chemical interaction between ozone and MWCNTs and gradually destroying MWCNTs.[59] On the other hand in SnC10, upon UV-illumination with a higher energy than the SnO_2 bandgap, electron–hole pairs are photo-generated and spatially separated in SnO_2 matrix-structure and, as a result, release chemisorbed oxygen by the photo-excited holes ($O_{2\,(ads)}^- + h^+ \rightarrow O_{2\,(gas)}$). Subsequently, the generated unpaired UV-excited electrons with enlarged lifetime cause such enhancement in photocurrent and conductivity.[52]

CONCLUSION

Modified sol–gel assisted synthesis was successfully employed in the synthesis of hybrid MWCNT/SnOx. The structural, morphological and thermal properties of the hybrid nanocomposites were characterized by XRD, SEM–EDX, HRTEM, and TGA. TGA analysis exhibited MWCNTs decomposition at lower temperature than reported in the literature ($\approx$ 375°C). The lower decomposition temperature was attributed to oxidation ability of the SnO_x component that assists in removing the carbon content at lower temperatures. XRD patterns confirmed the structure composition of both pure and the nanohybrid composites. The decrease of crystallinity in diffraction patterns of SnC10 and CSn10 nanocomposites is related to overlapping diffraction peaks of the carbon nanotubes and tin oxide and indicated good dispersing of metal oxide nanoparticles within the hollow cavity of MWCNTs, which results in shielding of the peaks of metal oxides by MWCNTs. These findings are further supported by the images of both scanning electron microscope and transition electron microscope images that showed that the average width of MWCNTs was about 15 nm,and the lengths extended to several microns while the SnO_x nanoparticles are homogeneously dispersed on the surface of CNTs in both of the two hybrid nanocomposite samples (CSn10, SnC10) with 5-nm average particle size. Prolonged exposure of hybrid nanocomposites-chitosan thin film to UV-radiation results in marked decreasing of the band gap as well as the absorption intensity in the 200–350 nm range indicating that the carbon nanotubes exhibit photo-induced oxidation of the nanotubes and structure sensitivity of these materials to UV radiation. Among all samples, SnC10 samples recorded the highest dielectric constant, which is about six times greater than CSn10 at 100 Hz. The introduction of either MWCNTs and SnO_x enhanced greatly the conductivity of each other. Compared with the undoped SnO_2 nanoparticles, the conductivity of SnO_x doped with 10% wt carbon nanotubes (SnC10) increased by a factor of 76 times, while CSn10 recorded the highest conductivity value (greater than MWCNTs by about 110 times) which could be related to: (1) The very low Schottky barrier between SnO_2 grains and MWCNTs. (2) Electrons conduct in the MWCNTs with low resistance. (3) The high aspect ratio structure and good conductivity of MWCNT-COOHs make them act as a bridge for electrons linking SnO_2 nanoparticles together. (4) The numerous p orbits of MWCNT-COOHs also can act as acceptor levers to improve the conductivity. Upon UV-illumination, electric conductivities of both SnC10 and CSn10 adopt a reverse response to the UV illumination and correspond to their element content. The electric conductivity decreasing in CSn10 could be related to that, in a rich oxygen environment, UV-radiation can prompt ozone formation, which induces a chemical interaction between ozone and MWCNTs and gradually destroying MWCNTs. On the other hand, UV-illumination of SnC10 with a higher energy than the tin oxide band gap leads to generation of electron–hole pairs that are spatially separated in SnO_2 matrix-structure and subsequently cause such enhancement in photocurrent and conductivity.

REFERENCES

1. P.C. Ma, N.A. Siddiqui, G. Marom, and J.K. Kim, *Compos. A Appl. Sci. Manuf.* 41, 1345 (2010).
2. N. V. Myung, S. Mubeen, A. Mulchandani and M. A. Deshusses, (Google Patents: 2016).
3. P.L. Gautherin, L. Sabaut, P. Ponard, J.P. Mazellier, P. Legagneux and S. Xavier, In *Vacuum Nanoelectronics Conference (IVNC), 2017 30th International*, (IEEE: 2017), pp 106–107.
4. S. Pillai, S. Motshekga, S. Sinha Ray, and J. Kennedy, *J. Nanomater.* 2012, 861591 (2012).
5. P. Liu, D. Zhou, C. Zhang, H. Wei, X. Yang, Y. Wu, Q. Li, C. Liu, B. Du, and L. Liu, *Nanotechnology* 29, 345601 (2018).
6. R. Rakhi, *Nanocarbon and its Composites* (Amsterdam: Elsevier, 2019), pp. 489–520.
7. R. Atchudan, B.G. Cha, N. Lone, J. Kim, and J. Joo, *Korean J. Chem. Eng.* 36, 157 (2019).
8. E.V. Lobiak, E.V. Shlyakhova, A.V. Gusel'nikov, P.E. Plyusnin, Y.V. Shubin, A.V. Okotrub, and L.G. Bulusheva, *Phys. Status Solidi (b)* 255, 1700274 (2018).
9. S. Ramesh, S. Khandelwal, K.Y. Rhee, and D. Hui, *Compos. B Eng.* 138, 45 (2018).
10. B. Siwach, S. Sharma, and D. Mohan, *J. Integr. Sci. Technol.* 5, 1 (2017).
11. S. Mallakpour and E. Khadem, *Chem. Eng. J.* 302, 344–367 (2016).
12. I. Kainthla, J.T. Bhanushali, R.S. Keri, and B.M. Nagaraja, *Catal. Sci. Technol.* 5, 5062 (2015).
13. A. Mittal, M. Naushad, G. Sharma, Z. ALothman, S. Wabaidur, and M. Alam, *Desalination and Water Treatment* 57, 21863 (2016).
14. A. Dey, *Mater. Sci. Eng. B* 229, 206 (2018).
15. W. Ke, D. Zhao, C. Xiao, C. Wang, A.J. Cimaroli, C.R. Grice, M. Yang, Z. Li, C.S. Jiang, and M. Al-Jassim, *J. Mater. Chem. A* 4, 14276 (2016).
16. W. Dong, J. Xu, C. Wang, Y. Lu, X. Liu, X. Wang, X. Yuan, Z. Wang, T. Lin, and M. Sui, *Adv. Mater.* 29, 1700136 (2017).
17. H. Jadhav, S. Suryawanshi, M. More, and S. Sinha, *Appl. Surf. Sci.* 419, 764 (2017).
18. S.B. Naghadeh, S. Vahdatifar, Y. Mortazavi, A.A. Khodadadi, and A. Abbasi, *Sens. Actuators B Chem.* 223, 252 (2016).
19. G. An, W. Ma, Z. Sun, Z. Liu, B. Han, S. Miao, Z. Miao, and K. Ding, *Carbon.* 45, 1795 (2007).
20. P. Kaushik, M. Eliáš, J. Prášek, Z. Pytlíček and L. Zajíčková, In *2018 IEEE Sensors* (IEEE: 2018), pp 1–3.
21. Q. Kuang, S.F. Li, Z.X. Xie, S.C. Lin, X.H. Zhang, S.Y. Xie, R.B. Huang, and L.S. Zheng, *Carbon* 44, 1166 (2006).
22. P.M. Korusenko, S.N. Nesov, V.V. Bolotov, S.N. Povoroznyuk, A.I. Pushkarev, K.E. Ivlev, and D.A. Smirnov, *Nucl. Instrum. Methods Phys. Res. Sect. B* 394, 37 (2017).
23. L. Aravinda, K. Nagaraja, H. Nagaraja, K.U. Bhat, and B.R. Bhat, *Nanotechnology* 27, 314001 (2016).
24. M. Sreekanth, S. Ghosh, P. Biswas, S. Kumar, and P. Srivastava, *Appl. Surf. Sci.* 383, 84 (2016).
25. M.A. Wahba and A.A. Badawy, *J. Sol Gel Sci. Technol.* 1, 1–11 (2019).
26. M.A. Wahba, W. Mohamed, and A.A. Hanna, *Int. J. Chem. Technol Res.* 9, 914 (2016).
27. J. Eom, H. Kwon, J. Liu, and O. Zhou, *Carbon* 42, 2589 (2004).
28. L. Zhao and L. Gao, *Carbon* 42, 1858 (2004).
29. A. Patterson, *Phys. Rev.* 56, 978 (1939).

30. I. Srikanth, N. Padmavathi, P. Prasad, P. Ghosal, R. Jain, and C. Subrahmanyam, *Bull. Mater. Sci.* 39, 41 (2016).
31. R. Das, M.E. Ali, S.B.A. Hamid, M. Annuar, and S. Ramakrishna, *J. Nanomater.* 2014, 237 (2014).
32. N.T. Abdel-Ghani, G.A. El-Chaghaby, and F.S. Helal, *J. Adv. Res.* 6, 405 (2015).
33. E. Edwards, E. Antunes, E.C. Botelho, M. Baldan, and E. Corat, *Appl. Surf. Sci.* 258, 641 (2011).
34. A. Mahajan, A. Kingon, A. Kukovecz, Z. Konya, and P.M. Vilarinho, *Mater. Lett.* 90, 165 (2013).
35. D. Bom, R. Andrews, D. Jacques, J. Anthony, B. Chen, M.S. Meier, and J.P. Selegue, *Nano Lett.* 2, 615 (2002).
36. D.Y. Kang, P. Pokharel, Y.S. Kim, S. Choi, and S.H. Choi, *J. Nanomater.* 16, 157 (2015).
37. Y.L. Liu, H.F. Yang, Y. Yang, Z.M. Liu, G.L. Shen, and R.Q. Yu, *Thin Solid Films* 497, 355 (2006).
38. W.H. Baur and A.A. Khan, *Acta Crystallogr. Sect. B: Struct. Crystallogr. Cryst. Chem.* 27, 2133 (1971).
39. J. Donaldson, W. Moser, and W. Simpson, *Acta Crystallogr. A* 16, 22 (1963).
40. V. Gupta and T.A. Saleh, *Carbon Nanotubes-From Research to Applications* (London: InTech, 2011).
41. V. Tallapally, T.A. Nakagawara, D.O. Demchenko, Ü. Özgür, and I.U. Arachchige, *Nanoscale* 10, 20296 (2018).
42. M.A. Wahba and S.M. Yakout, *J. Sol Gel. Sci. Technol.* 92, 628 (2019).
43. V. Tallapally, D. Damma, and S.R. Darmakkolla, *Chem. Commun.* 55, 1560 (2019).
44. P. Alafogianni, K. Dassios, S. Farmaki, S. Antiohos, T. Matikas, and N.-M. Barkoula, *Colloids Surf. A* 495, 118 (2016).
45. T. Savage, S. Bhattacharya, B. Sadanadan, J. Gaillard, T. Tritt, Y. Sun, Y. Wu, S. Nayak, R. Car, and N. Marzari, *J. Phys. Condens. Matter* 15, 5915 (2003).
46. M. Grujicic, G. Cao, A. Rao, T. Tritt, and S. Nayak, *Appl. Surf. Sci.* 214, 289 (2003).
47. G. Chakraborty, K. Gupta, D. Rana, and A.K. Meikap, *Adv. Nat. Sci. Nanosci. Nanotechnol.* 3, 035015 (2012).
48. M. Batzill and U. Diebold, *Prog. Surf. Sci.* 79, 474 (2005).
49. A.M. Ganose and D.O. Scanlon, *J. Mater. Chem. C* 4, 1467 (2016).
50. B. Choudhury and A. Choudhury, *Int. Nano Lett.* 3, 55 (2013).
51. N. Bafandeh, M. Larijani, A. Shafiekhani, M. Hantehzadeh, and N. Sheikh, *Chin. Phys. Lett.* 33, 117801 (2016).
52. J.R.D. Retamal, C.Y. Chen, K.Y. Lai, and J.H. He, *Handb. Zinc Oxide Rel. Mater. Vol. Two Dev. Nano-Eng.* 2, 133 (2012).
53. C.M. Mo, L. Zhang, and G. Wang, *Nanostruct. Mater.* 6, 823 (1995).
54. A.K. Chawla, D. Kaur, and R. Chandra, *Opt. Mater.* 29, 995 (2007).
55. N. Ponpandian, P. Balaya, and A. Narayanasamy, *J. Phys. Condens. Matter* 14, 3221 (2002).
56. M.J. Jiang, Z.M. Dang, M. Bozlar, F. Miomandre, and J. Bai, *J. Appl. Phys.* 106, 084902 (2009).
57. P. Barber, S. Balasubramanian, Y. Anguchamy, S. Gong, A. Wibowo, H. Gao, H. Ploehn, and H.-C. Zur Loye, *Materials* 2, 1697 (2009).
58. S.Z. Kang, Z. Cui, and J. Mu, *J. Dispers. Sci. Technol.* 28, 569 (2007).
59. D.B. Mawhinney, V. Naumenko, A. Kuznetsova, J.T. Yates, J. Liu, and R. Smalley, *J. Am. Chem. Soc.* 122, 2383 (2000).

Publisher's Note Springer Nature remains neutral with regard to jurisdictional claims in published maps and institutional affiliations.